Five Years of Neutrino Physics with Super-Kamiokande

M.B. Smy

for the Super-Kamiokande Collaboration

Department of Physics and Astronomy, 4182 Frederick Reines Hall, University of California, Irvine,
Irvine, California 92697-4575, USA

Using data from both solar and atmospheric neutrinos, Super-Kamiokande has provided fundamental information on neutrino flavor mixing and neutrino mass square differences.

1   Introduction

Both solar and atmospheric neutrino measurements have yielded significantly smaller interaction rates than expected: the reduction of the solar ν_e flux compared to the standard solar model (SSM[1]) was observed to be between 50%[2,3,4,5] and 65%[6,7], the atmospheric ν_e flux was found to be the same within uncertainty while the atmospheric ν_μ flux was measured at about 65% of the calculation[8]. Both deficits — known as the solar neutrino problem and the atmospheric anomaly — are explained by neutrino flavor changes caused by oscillations: solar neutrino experiments detect predominantly ν_e and atmospheric experiments are less sensitive to ν_τ interactions.

Neutrino oscillations require the physical mass eigenstates ν_i (with masses $m_1 < m_2 < ...$) to differ from the flavor eigenstates ν_α (defined by charged-current interactions with a charged lepton of flavor α). The flavor eigenstates ν_α are orthogonal linear combinations of the mass eigenstates ν_i: $\nu_\alpha = \sum_i U_{\alpha i} \nu_i$. U is the unitary mixing matrix. Since there are three charged lepton flavors (e, μ and τ), only three neutrino flavor eigenstates can produce charged leptons via charged-current interactions. The invisible width of the Z^0 boson is compatible with decay into three light neutrinos, so only three neutrino flavor eigenstates participate in neutral-current interactions. If there are more than three neutrinos (and therefore more than three neutrino flavor eigenstates), then some of the flavor eigenstates are "sterile", that is, they feel neither charged- nor neutral-current interactions. In case of just three neutrinos (and neglecting CP violating phases), the mixing matrix U can be described phenomenologically using the three mixing angles θ_{12}, θ_{13} and θ_{23}. Using the short notation $s_{ij} = \sin\theta_{ij}, c_{ij} = \cos\theta_{ij}$ the mixing

matrix becomes

$$U = \begin{pmatrix} c_{12}c_{13} & s_{12}c_{13} & s_{13} \\ -s_{12}c_{23} - c_{12}s_{23}s_{13} & c_{12}c_{23} - s_{12}s_{23}s_{13} & s_{23}c_{13} \\ s_{12}s_{23} - c_{12}c_{23}s_{13} & -c_{12}s_{23} - s_{12}c_{23}s_{13} & c_{23}c_{13} \end{pmatrix}$$

and the flavor conversion probability for a neutrino of energy E after flight distance L in vacuum is

$$P_{\text{vac}}(\nu_\alpha \longrightarrow \nu_\beta) = \delta_{\alpha\beta} - 4 \cdot \sum_{j<k} U_{\alpha j} U_{\beta j} U_{\alpha k} U_{\beta k} \sin^2 \frac{\Delta m_{jk}^2 L}{4E}$$

Atmospheric neutrino data requires [8] a Δm_{atm}^2 around 10^{-3}eV^2, while solar neutrino data implies a Δm_{sol}^2 below $\approx 10^{-4}\text{eV}^2 \ll \Delta m_{\text{atm}}^2$. For the purpose of this paper, the Δm_{sol}^2 is assumed to be Δm_{12}^2. Then, $\Delta m_{\text{atm}}^2 \approx \Delta m_{13}^2 \approx \Delta m_{23}^2$ and the atmospheric conversion probabilities are

$$
\begin{aligned}
P_{\text{vac}}(\nu_e \longrightarrow \nu_\mu) &\approx \sin^2 2\theta_{13} \sin^2 \theta_{23} \sin^2 \frac{\Delta m_{\text{atm}}^2 L}{4E} \\
P_{\text{vac}}(\nu_\mu \longrightarrow \nu_\tau) &\approx \left(\sin^2 2\theta_{\text{atm}} - \sin^2 2\theta_{13} \sin^2 \theta_{23}\right) \sin^2 \frac{\Delta m_{\text{atm}}^2 L}{4E} \\
P_{\text{vac}}(\nu_\tau \longrightarrow \nu_e) &\approx \sin^2 2\theta_{13} \cos^2 \theta_{23} \sin^2 \frac{\Delta m_{\text{atm}}^2 L}{4E} \\
P_{\text{vac}}(\nu_e \longrightarrow \nu_x) &\approx \sin^2 2\theta_{13} \sin^2 \frac{\Delta m_{\text{atm}}^2 L}{4E} \\
P_{\text{vac}}(\nu_\mu \longrightarrow \nu_x) &\approx \sin^2 2\theta_{\text{atm}} \sin^2 \frac{\Delta m_{\text{atm}}^2 L}{4E}
\end{aligned}
\tag{1}
$$

while the solar ν_e survival probability is

$$P_{\text{vac}}(\nu_e \longrightarrow \nu_e) \approx \cos^4 \theta_{13} \left(1 - \sin^2 2\theta_{\text{sol}} \sin^2 \frac{\Delta m_{\text{sol}}^2 L}{4E}\right) + \sin^4 \theta_{13} \tag{2}$$

with $\theta_{\text{sol}} = \theta_{12}$ and $\sin \theta_{\text{atm}} = \cos \theta_{13} \sin \theta_{23}$. Therefore, atmospheric neutrinos yield information about the last column of the mixing matrix and solar neutrinos about the first row. If θ_{13} is small, then both solar and atmospheric neutrinos can be analyzed using a two-neutrino model with effective solar and atmospheric mixing angles.

The characteristic L/E dependence of the vacuum oscillation probability is modified by the matter density along the flight path of the neutrino, since the coherent scattering amplitude of ν_e with matter is different from ν_μ or ν_τ, and sterile neutrinos don't undergo such coherent scattering at all. To take into account these matter effects, the potential V can be defined. The matter potential is the same for ν_μ and ν_τ, but differs for ν_e (or a sterile flavor). The same two-neutrino formulas may be used, with the substitution of

$$
\begin{aligned}
\left(\Delta m_{\text{mat}}^2\right)^2 &= \left(\Delta m^2\right)^2 \times \left[\left(\frac{2E\Delta V}{\Delta m^2} + \cos 2\theta\right)^2 + \sin^2 2\theta\right] \\
\sin^2 2\theta_{\text{mat}} &= \sin^2 2\theta \frac{\Delta m^2}{\Delta m_{\text{mat}}^2}
\end{aligned}
\tag{3}
$$

for Δm^2 and $\sin^2 2\theta$, where ΔV is the potential difference. While the vacuum conversion probabilities are invariant under $\theta \longrightarrow \pi/2 - \theta$ (that is $\sin 2\theta \longrightarrow \sin 2\theta$) the cos term changes sign ($\cos 2\theta \longrightarrow -\cos 2\theta$) and the effective Δm^2 and mixing changes. Therefore the "mirror symmetry" around maximal mixing ($\theta = \pi/4$) is broken by the matter effects. Depending on the sign of ΔV, a resonance can occur [9] which leads to a large conversion probability, even if the vacuum mixing is small.
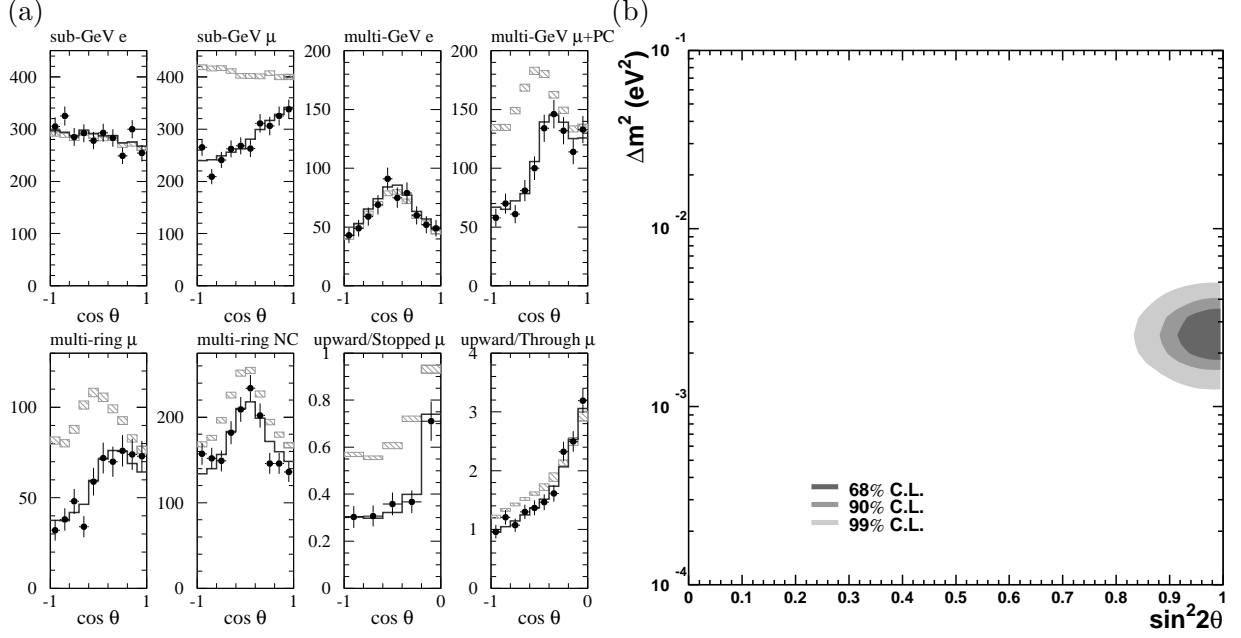
Figure 1: SK Atmospheric Neutrino Data and Atmospheric Neutrino Oscillation Parameters. (a) The upper four panels show the zenith angle distribution of single ring events for fully contained e-like rings (panel one and three), fully contained μ-like rings (panel two) and higher energy μ-like rings (panel four). In the lower row, panel one (brightest ring is μ-like) and two (brightest ring is e-like: neutral-current enhanced sample) contain the zenith angle distributions of the multi-ring samples. The zenith angle distributions of ν_μ interacting in the rock below SK are given in panel three (lower energy) and four (higher energy). The predictions of the atmospheric neutrino Monte Carlo calculation are overlaid (light-gray hatched areas). The best oscillation fit is indicated by the dark-gray solid line. (b) Allowed oscillation parameters for a two-neutrino fit assuming pure $\nu_\mu \leftrightarrow \nu_\tau$ oscillations.

2 Atmospheric Neutrinos

Atmospheric neutrinos originate when primary cosmic rays strike the earth's atmosphere and produce a shower of pions, which decay into muons and ν_μ's. Each muon decay produces a ν_e as well as a ν_μ. Super-Kamiokande (SK) is a cylindrical 50,000 ton water Cherenkov detector. An optical barrier separates an "inner" concentric cylinder from the outer "anti-counter". The inner cylinder (32,000 tons) is viewed by 11,146 inward-facing 20" photomultiplier tubes, the outer cylinder by 1885 outward-facing 8" photomultiplier tubes. SK uses the anti-counter (which surrounds the inner detector) to define "fully contained events" (no entering or exiting charged particles), "partially contained events" (only exiting charged particles) and "entering events". In each case, the direction of a charged particle is reconstructed using the directionality of the Cherenkov light.

Cherenkov rings are predominantly produced by electrons and muons. The Cherenkov ring produced by electrons typically has a "fuzzy" outer edge due to electromagnetic showers. A muon, on the other hand, does not shower as much, and therefore its Cherenkov ring has a "sharp" outer edge. This allows the construction of a particle identification likelihood (PID) which distinguishes "e-like" from "μ-like" events. The energy of fully contained events is measured using the amount of produced Cherenkov light. The sample is split into a "sub-GeV" and a "multi-GeV" sample. If the brightest ring in an event containing several Cherenkov rings is μ-like, the event is most likely due to a ν_μ charged-current interaction. Since the decay photons of neutral pions produce electrons by Compton scattering, a neutral-current enhanced multi-ring sample can be defined using the PID and the π^0 invariant mass.

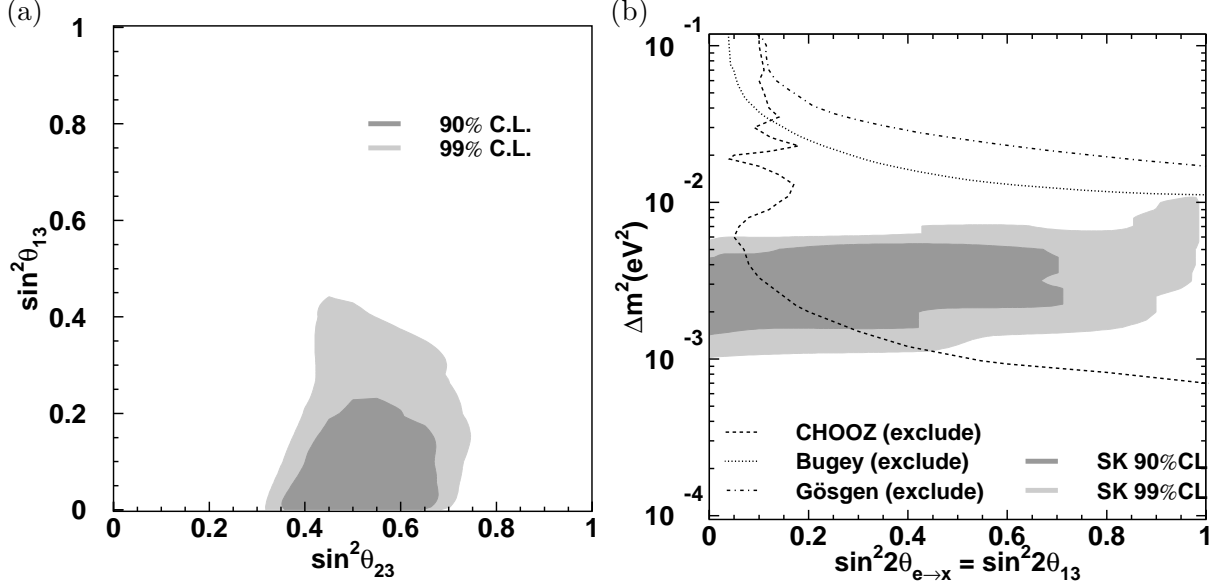Partially contained events are almost always due to higher energy muons. The energy of

Figure 2: Neutrino Mixing with Three Parameters. (a) Allowed area of $\sin^2 \theta_{13}$ and $\sin^2 \theta_{23}$. At 90% C.L. SK data allows up to about 40% of e-type content of the atmospheric oscillation. (b) Allowed range of the atmospheric ν_e disappearance probability compared to the limits for $\overline{\nu_e}$ obtained from various reactor experiments. The most stringent limit comes from the CHOOZ experiment.

those muons can only be estimated statistically using Monte Carlo distributions. Upward-going entering events are due to the interaction of ν_μ in the rock below SK. If the "upward-going muons" stop inside the detector ("upward/stopped"), then the average energy of the producing ν_μ's is lower than for upward-going muons which enter and exit the detector ("upward/through").

The direction of low energy leptons yield little information about the neutrino's direction (and in turn its flight distance). However, the zenith angle θ of high energy leptons is correlated with the neutrino flight distance L. SK has accumulated 1289 live days of atmospheric neutrino data using a fiducial volume of 22,500 tons. The zenith distributions of electrons (see figure 1) show good agreement with the Monte Carlo based on the atmospheric neutrino flux calculation. However, there are significantly less muons than expected. Downward-going ($\cos \theta = 1$) atmospheric neutrino-induced (multi-GeV) μ-like events agree with the Monte Carlo, upward-going events show the strongest deficit. A similar distortion is seen in the multi-ring μ-like sample, but not in the multi-ring neutral-current enhanced sample. Upward-going through-going muons agree with Monte Carlo in the horizontal direction, but are suppressed at $\cos \theta = -1$. There are less upward-going stopped muons than expected. As seen in figure 1 (a) oscillations of ν_μ's into ν_τ's are able to explain all the zenith angle distributions. The same figure also gives allowed ranges for neutrino mixing and Δm^2. The data prefer maximal mixing and $\Delta m^2 \approx 2$–$3 \cdot 10^{-3} \mathrm{eV}^2$.

Due to the lack of an e-like appearance signal, $\nu_\mu \leftrightarrow \nu_e$ oscillations are disfavored compared to $\nu_\mu \leftrightarrow \nu_\tau$. However, any e-like appearance due to $\nu_\mu \to \nu_e$ is unfortunately washed out by a disappearance due to $\nu_e \to \nu_\mu$, so the SK data allow a substantial "ν_e" component (about 40% at 90% C.L.) in the ν_μ oscillations. Figure 2 shows the allowed values for both θ_{13} and θ_{23} (according to equation (1) θ_{12} plays no role for atmospheric neutrino oscillations) in a three-neutrino oscillation analysis. Maximal mixing for θ_{23} and zero mixing for θ_{13} is preferred. The same figure also gives allowed ranges for $\Delta m^2_{\mathrm{atm}}$ and the "disappearance probability" $\sin^2 2\theta_{13}$. More stringent limits on this probability come from the CHOOZ reactor experiment [10].

Four-neutrino oscillations are investigated for the case of $\theta_{13} = 0$ and a Δm^2 hierarchy ($\Delta m^2_{\mathrm{LSND}} \approx 1\mathrm{eV}^2 \gg \Delta m^2_{\mathrm{atm}} \approx 10^{-3}\mathrm{eV}^2 \gg \Delta m^2_{\mathrm{sol}} \approx 10^{-4}\mathrm{eV}^2$). The "content" of the fourth flavor (sterile neutrino) in atmospheric neutrino oscillations can be parameterized by
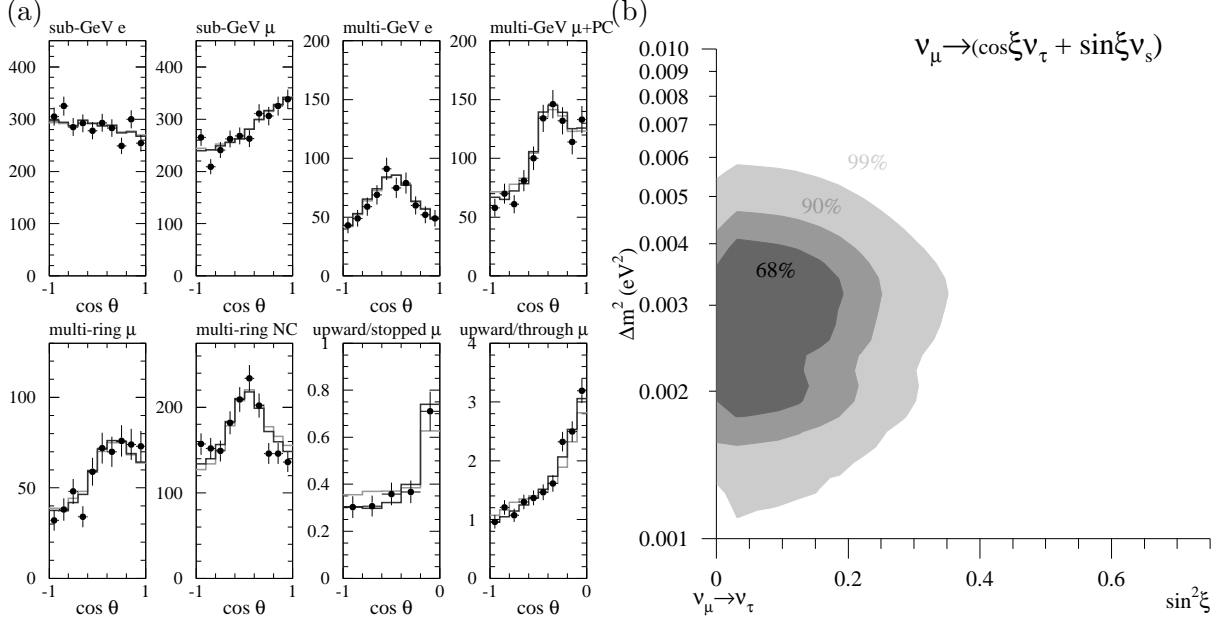
Figure 3: Limit on Sterile Content of Atmospheric Neutrino Oscillations. (a) Pure $\nu_\mu \leftrightarrow \nu_\tau$ (solid black line) fits the upward-going μ zenith distribution better than pure $\nu_\mu \leftrightarrow \nu_s$ (solid gray line) because of matter effects. For the same reason, there is also a small difference in the high energy μ-like events. The neutral-current enhanced multi-ring sample shows no hint for a disappearance of active flavors and therefore favors pure $\nu_\mu \leftrightarrow \nu_\tau$. (b) The limit on the sterile content is $\sin^2 \xi < 0.25$ at 90% C.L.

$\sin^2 \xi$: $\nu_\mu \rightarrow (\cos \xi \nu_\tau + \sin \xi \nu_s)$. Figure 3 compares the best pure $\nu_\mu \rightarrow \nu_\tau$ fit with the best pure $\nu_\mu \rightarrow \nu_s$ fit and gives the allowed ranges for $\Delta m^2_{\mathrm{atm}}$ and $\sin^2 \xi$. In case of purely sterile oscillations, matter effects reduce the conversion probability for high energy neutrinos which affects the upward-going muon samples, the partially contained events, and the multi-GeV μ-like events. The neutral-current enhanced multi-ring zenith angle distribution becomes up/down asymmetric, since sterile neutrinos don't interact via neutral currents. In every case, data disfavors the purely sterile case. Data likes best zero sterile content At 90% C.L., the maximum allowed sterile content is 25%. The range of Δm^2 is consistent with the other fits.

Other hypotheses to explain the SK zenith angle distributions are investigated as well. The conversion probability is parameterized as follows: (i) $\sin^2 2\theta \sin^2(\alpha L \times E)$ ("LxE"), (ii) $\sin^4 \theta + \cos^4 \theta \left(1 - e^{-\alpha L/E}\right)$ ("ν_μ decay") and (iii) $\left(\sin^2 \theta + \cos^2 \theta e^{-\alpha L/E}\right)^2$ ("ν_μ decay to ν_s"). Table 1 gives a summary of all investigated hypotheses. $\nu_\mu \rightarrow \nu_\tau$ is strongly favored by the data.

Table 1: Comparison of Several Flavor Conversion Hypotheses. $\nu_\mu \rightarrow \nu_\tau$ is strongly favored by the data.

Mode	best fit parameters		$\Delta\chi^2$	#σ
$\nu_\mu \rightarrow \nu_\tau$	$\sin^2 2\theta = 1.00$	$\Delta m^2 = 2.5 \cdot 10^{-3}\mathrm{eV}^2$	0.0	0.0
$\nu_\mu \rightarrow \nu_e$	$\sin^2 2\theta = 0.97$	$\Delta m^2 = 5 \cdot 10^{-3}\mathrm{eV}^2$	79.3	8.9
$\nu_\mu \rightarrow \nu_s$	$\sin^2 2\theta = 0.96$	$\Delta m^2 = 3.6 \cdot 10^{-3}\mathrm{eV}^2$	19.0	4.4
LxE	$\sin^2 2\theta = 0.90$	$\alpha = 5.3 \cdot 10^{-4}/(\mathrm{GeVkm})$	67.1	8.2
ν_μ decay	$\cos^2 \theta = 0.47$	$\alpha = 3.0 \cdot 10^{-3}\mathrm{GeV/km}$	81.1	9.0
ν_μ decay to ν_s	$\cos^2 \theta = 0.33$	$\alpha = 1.1 \cdot 10^{-2}\mathrm{GeV/km}$	14.1	3.8

If atmospheric ν_μ indeed oscillate into ν_τ, then about 80 ν_τ charged-current events are expected in the SK data set. The high threshold for this reaction makes it difficult to isolate these events. At this energy, atmospheric neutrinos typically produce a spray of particles,
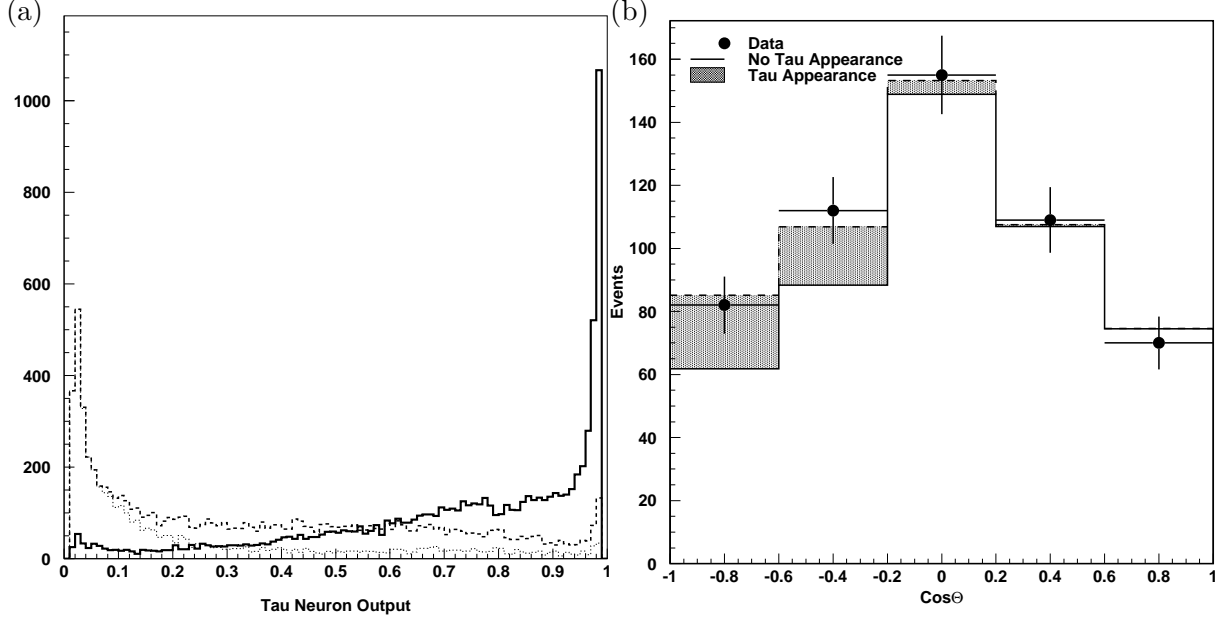
Figure 4: Search for Tau Appearance. (a) Neural net output for atmospheric ν_μ charged-current interaction Monte Carlo (dotted line), all atmospheric ν Monte Carlo without ν_τ (dashed line) and tau Monte Carlo (solid line). Since there is only a small number of tau events expected in the SK data, the analysis is limited by background from other atmospheric ν-induced events. (b) Fit to the zenith angle distribution of the tau-enriched sample. Tau events are only expected in the upward direction. Data favors tau appearance at about the 2σ level.

and ring-counting becomes very difficult. One analysis abandons ring-counting altogether and reconstructs the amount of "energy flow" as a function of direction based on the angular light distribution. From the energy flow, jet variables are formed. A τ likelihood function combines such variables to discriminate between τ events and other atmospheric neutrino interactions. Another analysis constructs a similar τ likelihood from variables based on the conventional event reconstruction (ring-counting) A third analysis utilizes a neural net to combine similar ring-counting variables. Figure 4 (a) explains the output of the "tau neuron" when tested on Monte Carlo. In spite of the good separation between tau and non-tau events, the analysis (like the other two) is limited by background, since there are much fewer tau events than non-tau events. The same figure shows the zenith angle distribution of the tau-enriched sample (using the tau neuron). An excess of about two sigma (see also table 2) is observed for upward-going events.

Table 2: Results of Three τ Appearance Searches.

Analysis	Number of τ-Events in Fit	Efficiency	Observed,	Expected Signif.
Energy-Flow	79^{+44}_{-40}(stat+syst)	32%	1.8σ	1.9σ
Ring-Counting	66 ± 41(stat)$^{+25}_{-18}$(syst)	43%	1.5σ	2.0σ
Neural Net	92 ± 35(stat)$^{+18}_{-23}$(syst)	51%	2.2σ	2.0σ

3   Solar Neutrinos

SK observes solar neutrinos via elastic neutrino-electron scattering. Only solar neutrinos with fairly high energy (several MeV) can be detected. These neutrinos originate from the β^+-decay of ^{8}B or the ^{3}He-proton (*hep*) fusion reaction. Like other experiments SK found a deficit of solar
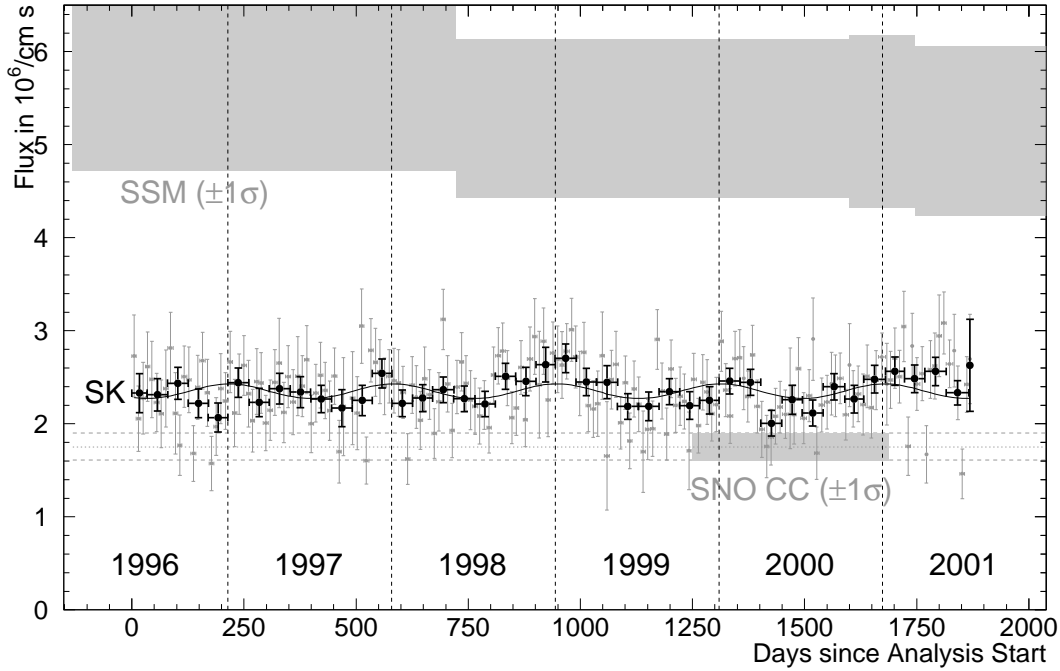
Figure 5: Time Variation of the Neutrino Flux Inferred from the Elastic Scattering Rate. The black points show the elastic scattering rate in SK during 1.5 months. The gray points extend over a time period of 10 days. Each black point is significantly below the SSM prediction and above the SNO charged-current rate. The solid line shows the 7% flux variation which is expected from the 3.5% change in the distance between the sun and the earth.

neutrinos; all such deficits are explained by solar neutrino oscillations. Since event times are recorded and the event energy is reconstructed, SK can search for time variations and an energy dependence of the rate deficit.

The solar neutrino flux is inferred from the SK interaction rate assuming only ν_e's. The large solar neutrino event sample collected by SK during 1496 live days inside a fiducial volume of 22,500 tons enables a precise study of the time-dependence of this flux. The gray data points in figure 5 contain only 10 days of data. The flux measured in each of these 185 time bins is significantly smaller than the SSM prediction. Also shown are the larger 1.5 month time bins (black data points). At first glance, the flux looks constant. A more careful study reveals an indication for a periodic change with a one year period. Since the sun is a neutrino point source, a 7% change of that kind is expected by the 3.5% change in distance between the sun and the earth (see solid black line of figure 5). If the 1.5 month data points are combined into 8 "seasonal" bins, a χ^2 test to this 7% variation yields $\chi^2 = 4.7$ (69% C.L.) compared to $\chi^2 = 10.3$ (17% C.L.) for a constant flux. The difference in χ^2 corresponds to about 2.5 sigma. There is no hint of other long-term time variations (e.g. arising from the oscillation phase).

The charged-current interaction rate measured by the SNO experiment explores the solar neutrino flux in a similar energy range and can therefore be compared directly. The flux measured by SK in each of the 42 (1.5 month) time bins is significantly larger then the flux measured by SNO. Solar neutrino oscillations of ν_e into other, active flavors predict such an excess of the elastic scattering rate over a charged-current measurement; that excess is due to a larger neutral-current amplitude in the elastic-scattering process. The discrepancy between the SK and the SNO neutrino flux measurement is therefore interpreted as evidence for the presence of other active flavors than ν_e in the solar neutrino flux.
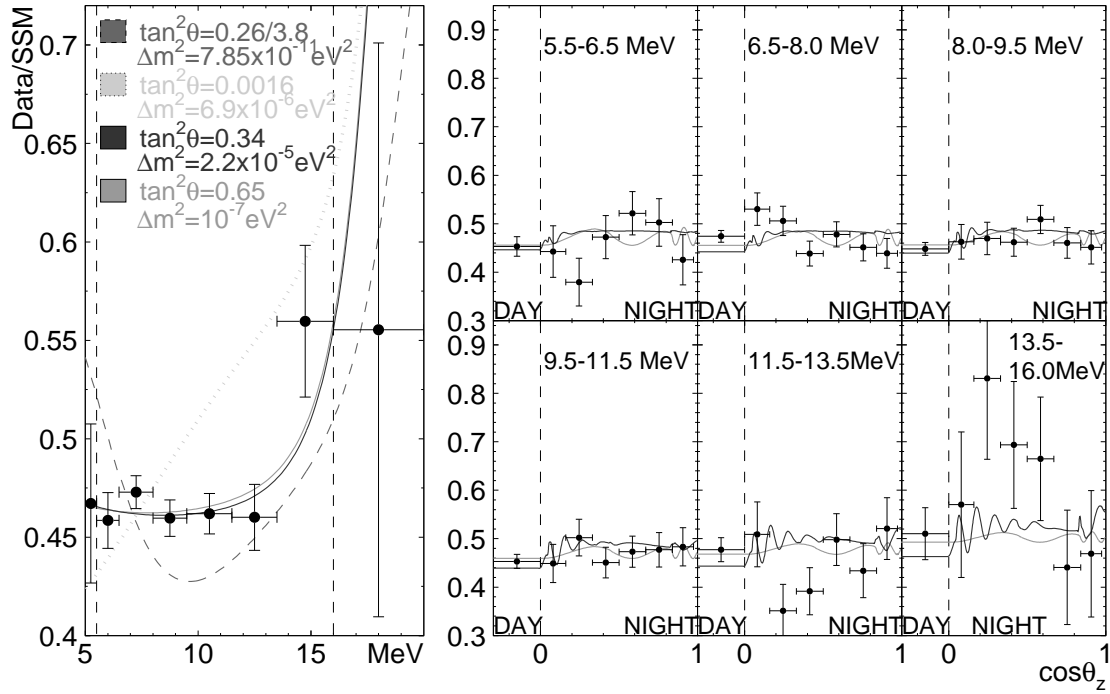
Figure 6: Zenith Spectrum and Four Oscillation Predictions. SMA (dotted line) and VAC (dashed line) solutions are disfavored by spectral distortion data, LOW (light gray) solutions by the absence of solar zenith angle variation. The LMA solutions (dark gray) fit best.

Depending on the solar Δm^2, solar neutrino oscillations can be driven by the oscillation phase or by matter effects. Strong spectral distortions are expected in the former case. In the latter case, spectral distortions can still occur as a consequence of a (energy-dependent) resonance caused by the sun's matter density. The earth's matter density can also affect the conversion probability resulting in most cases in a "regeneration" of "disappeared" ν_e's during the night. SK searches for both effects with the "zenith angle spectrum" (see figure 6): The data is broken into eight energy bins (according to the SK energy resolution). Between 5.5 and 16 MeV of reconstructed energy, SK has collected a sufficiently large number of solar neutrino candidate events to subdivide each energy bins in seven solar zenith angle (θ_z) bins. In each bin, the ratio of the observed event rate and the rate expected by the SSM is shown. Neither spectral distortion nor a regeneration effect is evident in the data.

For the oscillation analysis [11,12] of this zenith angle spectrum (and other solar data), θ_{13} is set to zero in equations (2). This is justified by the lack of evidence for a positive θ_{13} in either atmospheric neutrino data from SK or reactor neutrino data from CHOOZ. Analysis of the data from the other SK experiments reveal several distinct allowed areas shown in light-gray in figure 7 (a) which are referred to as "solutions" to the solar neutrino problem. The small mixing angle solution (SMA) is the only one with a small solar mixing angle. There are three large angle solutions. The large mixing angle solution (LMA) has the largest Δm^2 and the vacuum solution (VAC) the smallest. The lower part of the region extended between 10^{-9}eV^2 and 10^{-7}eV^2 is called quasi-VAC solution, the upper part is the LOW solution. Figure 6 shows the typical spectral and solar zenith angle behavior of the main four solutions. The absence of spectral distortions excludes VAC and SMA, the absence of the nightly "regeneration shape" required by the LOW solution disfavors this solution as well. Figure 7 (a) shows the excluded regions of parameter space due to only the shape of the zenith angle spectrum (gray areas). Only LMA
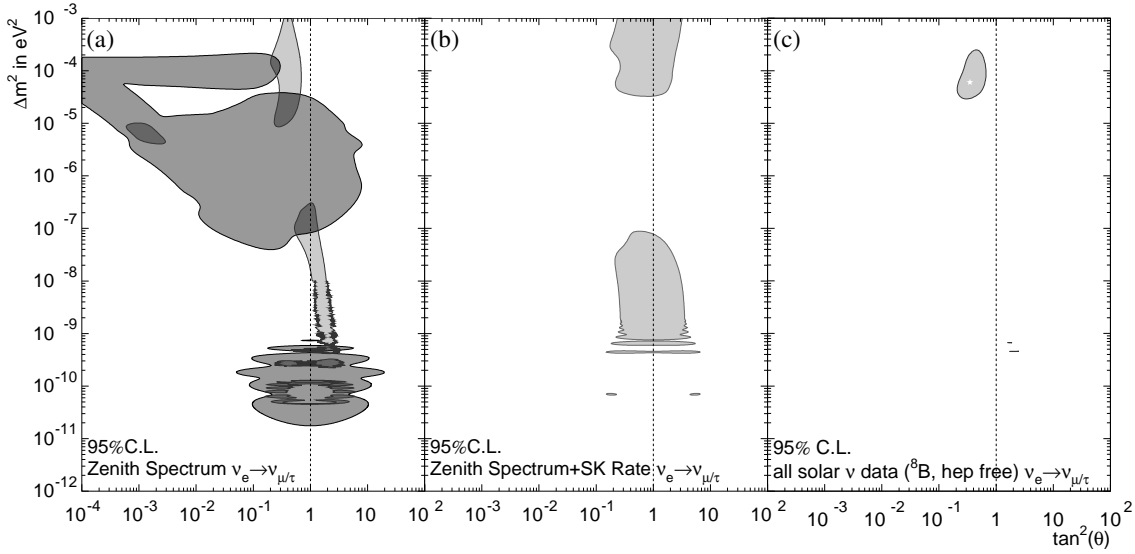
Figure 7: Solar Neutrino Oscillation Parameters. (a) The gray area is excluded at 95% C.L. by the shape of the SK zenith angle spectrum, the light-gray area is allowed by data from Gallex/GNO, SAGE, Homestake and SNO. The overlap of both is shaded dark-gray. (b) The light-gray area is allowed by the shape of the SK zenith angle spectrum and the SK interaction rate using the SSM prediction of the ^{8}B flux. (c) The light-gray area is allowed using all solar neutrino data. The SSM predictions of the ^{8}B and *hep* flux are not used. The best fit (located in the LMA solution) is marked by the white asterisk.

and quasi-VAC solutions remain allowed. Combining the shape of the zenith angle spectrum with the SK rate measurement, only the two allowed regions in figure 7 (b) remain (LMA and quasi-VAC). SK solar neutrino data by itself requires large mixing and prefers maximal mixing. Stronger constrains are obtained when the data of the other solar neutrino experiments are used in addition to SK data. The quasi-VAC solution is rejected by the rates of all experiments. Combining [12] SK zenith angle spectrum and rate with the rates of all other solar neutrino experiments, SK found for the first time a *unique* solution, the LMA solution, at $\approx$95% C.L. Figure 7 (c) shows the allowed range in mixing and Δm^2. The mixing is large but not maximal and Δm^2 is somewhat smaller then 10^{-4}eV^2. Since SK spectral data limits high energy solar neutrino spectral distortions to be small, the combination of the SK rate and the charged-current rate of either the Homestake experiment or SNO forbids a purely sterile solar neutrino oscillation solution.

4 Neutrino Mixing and Masses

Figure 8 summarizes and combines the current best knowledge of neutrino masses and mixing from solar and atmospheric neutrino data. There are no hints for sterile neutrinos in either atmospheric or solar neutrino oscillations, so three neutrinos are sufficient to explain both data sets. The mass spectrum of figure 8 is for the hierarchical case, that is m_1 is much smaller than the other masses, and the mass eigenstate pair responsible for solar neutrino oscillations is m_1 and m_2. CP violating phases are neglected. The displayed values of θ_{ij} are the best-fit values from the atmospheric and the solar oscillation analyses.
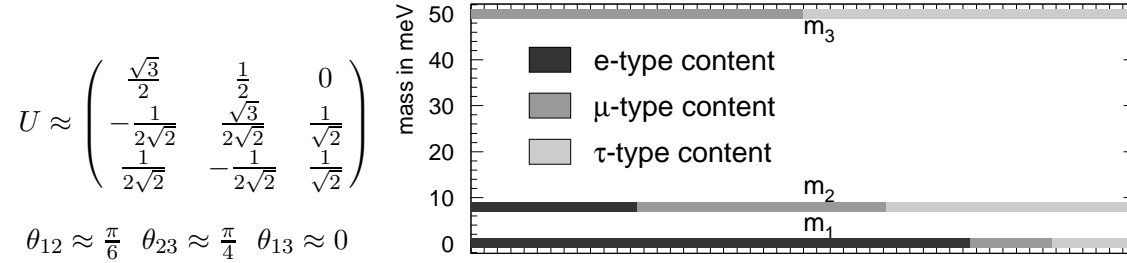
$$U \approx \begin{pmatrix} \frac{\sqrt{3}}{2} & \frac{1}{2} & 0 \\ -\frac{1}{2\sqrt{2}} & \frac{\sqrt{3}}{2\sqrt{2}} & \frac{1}{\sqrt{2}} \\ \frac{1}{2\sqrt{2}} & -\frac{1}{2\sqrt{2}} & \frac{1}{\sqrt{2}} \end{pmatrix}$$

$$\theta_{12} \approx \frac{\pi}{6} \quad \theta_{23} \approx \frac{\pi}{4} \quad \theta_{13} \approx 0$$

Figure 8: A Possible Leptonic Mixing Matrix U and Neutrino Mass Spectrum. The mixing matrix neglects CP violation and assumes that θ_{13} is indeed zero and the atmospheric mixing is maximal. The mass spectrum additionally assumes, that m_1 is small enough to be negligible and that the masses of the "solar pair" are smaller than the third mass. (hierarchical case).

Acknowledgments

References

1. J.N. Bahcall, M.H. Pinsonneault, S. Basu, *Astrophys. J.* **555**, 990 (2001).
2. Y. Fukuda et al., *Phys. Rev. Lett.* **77**, 1683 (1996).
3. E. Bellotti, *Nucl. Phys.* B*(Proc. Suppl.)* **91**, 44 (2001);
   W. Hampel et al., *Phys. Lett.* B **388**, 364 (1996);
   P. Anselmann et al., *Phys. Lett.* B **342**, 440 (1995).
4. V. Gavrin, *Nucl. Phys.* B*(Proc. Suppl.)* **91**, 36 (2001);
   J.N. Abdurashitov et al., *Phys. Lett.* B **328**, 234 (1994).
5. S. Fukuda et al., *Phys. Rev. Lett.* **86**, 5651 (2001).
6. B.T. Cleveland et al., *Astrophys. J.* **496**, 505 (1998).
7. Q.R. Ahmad et al. *Phys. Rev. Lett.* **87**, 71301 (2001).
8. Y. Fukuda et al., *Phys. Rev. Lett.* **81**, 1562 (1998).
9. S.P. Mikheyev and A.Y. Smirnov, *Sov. Jour. Nucl. Phys.* **42**, 913 (1985);
   L. Wolfenstein, *Phys. Rev.* D **17**, 2369 (1978).
10. M. Apollonio, *Phys. Lett.* B **466**, 415 (1999).
11. S. Fukuda et al., *Phys. Rev. Lett.* **86**, 5656 (2001).
12. Details of this analysis and the full Super-Kamiokande-I solar neutrino data are found in:
    M. Smy, *hep-ex/0202020*; to be published in the proceedings of *Neutrino Oscillations and their Origin 2001*